JACS
JOURNAL OF THE AMERICAN CHEMICAL SOCIETY
Article
pubs.acs.org/JACS

Specific Ion Effects in Amphiphile Hydration and Interface Stabilization

Rüdiger Scheu,[†] Yixing Chen,[†] Hilton B. de Aguiar,[†] Blake M. Rankin,[‡] Dor Ben-Amotz,[‡] and Sylvie Roke*[,†]

[†]Laboratory for Fundamental BioPhotonics (LBP), Institute of Bio-Engineering (IBI), School of Engineering (STI), École Polytechnique Fédérale de Lausanne (EPFL), Station 17, CH-1015 Lausanne, Switzerland

[‡]Department of Chemistry, Purdue University, 560 Oval Drive, West Lafayette, Indiana 47907, United States

Supporting Information

ABSTRACT: Specific ion effects can influence many processes in aqueous solutions: protein folding, enzyme activity, self-assembly, and interface stabilization. Ionic amphiphiles are known to stabilize the oil/water interface, presumably by dipping their hydrophobic tails into the oil phase while sticking their hydrophilic head groups in water. However, we find that anionic and cationic amphiphiles adopt strikingly different structures at liquid hydrophobic/water interfaces, linked to the different specific interactions between water and the amphiphile head groups, both at the interface and in the bulk. Vibrational sum frequency scattering measurements show that dodecylsulfate (DS^-) ions do not detectably perturb the oil phase while dodecyltrimethylammonium (DTA^+) ions do. Raman solvation shell spectroscopy and second harmonic scattering (SHS) show that the respective hydration-shells and the interfacial water structure are also very different. Our work suggests that specific interactions with water play a key role in driving the anionic head group toward the water phase and the cationic head group toward the oil phase, thus also implying a quite different surface stabilization mechanism.

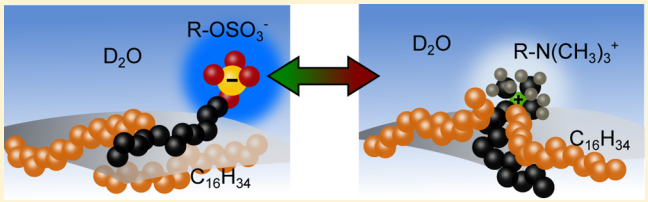

INTRODUCTION

Specific ion effects occur in many biological and chemical phenomena, such as protein folding, enzyme activity, bacterial growth, transport across membranes, and colloidal assembly.[1−5] The biological relevance of such specific ion effects is undoubtedly linked to the fact that living systems consist of macromolecules and assemblies that contain not only hydrophilic (polar and ionic) groups, but also extended hydrophobic (hydrocarbon) domains. Thus, to investigate specific ion interactions of relevance to such multiscale systems, we compare how different amphiphiles interact with water and oil/water interfaces. More specifically, we focus on single chain amphiphiles of similar structure, but either with negatively ($-OSO_3^-$) or positively ($-N(CH_3)_3^+$) charged head groups. We use oil nanodroplets in water, since such a system enables the in situ preparation of a large amount of clean[6,7] oil/water interface (~3000 cm^2/mL). We find that the head groups mentioned above not only interact very differently with bulk water molecules (as confirmed by Raman multivariate curve resolution, Raman-MCR, spectroscopy), but also have a strikingly different influence on interfacial oil and water structure (as evidenced by second harmonic scattering, SHS, and sum frequency scattering, SFS). More specifically, we find that the amphiphiles with the $-OSO_3^-$ head group do not detectably change the conformation of the interfacial oil chains and that they enhance the orientational order of surface water molecules, while those with the $-N(CH_3)_3^+$ head group strongly change the conformation of the interfacial oil chains and reduce the directionality of interfacial water molecules. Thus, the specific nature of the interaction of the ionic head groups with both water and oil evidently has a major impact on the structure of such complex interfaces.

Here, we first describe the differences in the hydration-shell of isolated octylsulfate (OS^-) and octyltrimethylammonium (OTA^+) ions obtained with Raman solvation shell spectroscopy. Then, we describe the vibrational sum frequency scattering measurements that were used to determine the structure of dodecylsulfate (DS^-) and dodecyltrimethylammonium (DTA^+) ions on impenetrable solid nanoparticles and penetrable liquid oil nanodroplets in water. By deuterating the oil phase, we selectively measure the conformation of the amphiphile's alkyl chains. This is followed by a study of the change in hydrophobic oil conformation at the nanodroplet/amphiphile/water interface upon adsorption of amphiphiles with deuterated alkyl chains. Finally, we describe the change in charge and in interfacial water structure induced by DS^- and DTA^+. We end with some remarks regarding applications and surface stabilization.

RESULTS AND DISCUSSION

Hydration-Shell Structure. Raman-MCR[8] is used to decompose experimental spectra into solvent and solute-correlated (SC) components. The SC spectrum contains

Received: November 25, 2013
Published: January 9, 2014

   dx.doi.org/10.1021/ja4120117 | J. Am. Chem. Soc. 2014, 136, 2040−2047

spectral information about the hydration-shell of the solute: It includes the vibrational modes of the solute itself, as well as water molecules that are perturbed by the solute, and thus differ from bulk water molecules. Raman-MCR has previously been used to detect water structure changes around hydrophobic[9−12] and ionic[13] solutes, as well as hydrophobic and specific ion[14b] interactions. Here, we report results obtained by using Raman-MCR to reveal differences between the hydration-shell structures of OS^- and OTA^+ surfactants dissolved in water, below the surfactant critical micelle concentration (cmc). Note that the cmc values for octyltrimethylammonium bromide (OTAB) and sodium octylsulfate (SOS) are both ∼130 mM.[15] Raman-MCR could not be used to probe the hydration-shell of isolated DTA^+ and DS^-, because solutions below the corresponding cmc values of 8.1, and 15 mM, respectively,[15] are below the detection limit of the Raman-MCR method.

Figure 1 shows the SC (hydration-shell) spectra of the OH-stretch region of 0.1 M solutions of OS^- ions (solid blue curve)

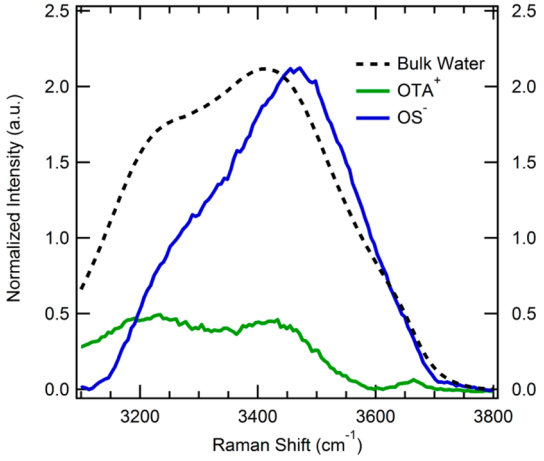

Figure 1. Amphiphile ion hydration. SC (hydration-shell) spectra of octylsulfate ions (OS^-) and octyltrimethylammonium (OTA^+) ions obtained using Raman-MCR. The solute-correlated spectra are normalized to the respective CH stretches of the surfactant ions, displaying the OH-stretch vibrational response of water surrounding the surfactant ions. The black dashed line depicts the OH Raman band of bulk water (scaled to the same height as the OS^- hydration-shell OH band).

and OTA^+ ions (solid green curve), each normalized to the surfactant CH band area. These OH stretch bands clearly differ significantly from each other, as well as from the OH band of bulk water (dashed black curve), as a result of amphiphile-induced water structure changes. The contribution from the Br^- counterion of OTA^+ has been removed by including an equal concentration of NaBr in the surfactant-free water reference spectrum, as previously described.[14b] Note that Na^+ ions have no observable effect on the water OH band,[13] and so no such procedure was required to correct for the Na^+ counterion of OS^-. Thus, the OTA^+ and OS^- spectra in Figure 1 arise only from the hydration-shell of the surfactant itself, with little or no contribution from the corresponding counterion. Differences between the spectra are due primarily to the different head groups, since the alkyl tails are of equal length (and similar results are obtained for surfactants with shorter tails, and the same head groups).

The hydration-shell spectrum of OTA^+ consists of two lobes, peaked at ∼3250 and ∼3450 cm^{-1}. The OTA^+ OH spectrum has a more prominent lower frequency OH stretch lobe than the bulk water spectrum, indicating that there is enhanced tetrahedral ordering of water molecules around the OTA^+ ions, as previously observed in the hydration-shells of nonpolar groups, such as the hydrophobic tails of alcohols (including neopentanol) and of tetraalkylammonium ions (including tetramethylammonium).[11,12] The small peak at ∼3660 cm^{-1} is due to an increase in the number of free (dangling) OH groups in the hydration-shell of OTA^+ (again as previously observed in aqueous alcohol and tetraalkylammonium solutions).[9,12] The hydration-shell spectrum of OS^- ions is more intense and looks quite different, as it is likely dominated by water OH groups that are H-bonded to the anionic sulfate head group, as a similar SC OH band is seen in the hydration-shells of halide anions,[13] as well as the SC spectra of aqueous sulfate ions. Thus, the differences between OS^- and OTA^+ hydration-shell spectra are consistent with the formation of hydrogen bonds between water and the sulfate head group, while the OTA^+ head group has a hydration-shell structure that is similar to that around neutral hydrophobic solutes that are not hydrogen bonded to water. We now turn to the molecular structure of the surfactant stabilized oil/water interface.

Interfacial Conformation. Surfactants at the planar oil/water interface have been studied with various methods including neutron scattering, X-ray scattering, and sum frequency (SF) generation.[16−25] The molecular surface structure of the nanoscopic oil droplet/water interface has received much less attention. Recent developments that combine light scattering and second-order nonlinear optics[26] have opened up the possibility to retrieve molecular structure and conformation from nanoparticle/droplet interfaces in water. Apart from providing molecular level details to the nanomaterial, it also increases the detection sensitivity for liquid interfaces and reduces impurity issues that are always linked to surface studies.[6] The surface composition of nanodroplets can be measured with vibrational sum frequency scattering (SFS), a vibrational coherent surface spectroscopy that measures the combined IR and Raman spectrum of molecules in non-centrosymmetric environments such as interfaces.[27−30] Selective deuteration allows to independently probe both the surfactant and the oil molecules, since C−D and C−H modes vibrate at different frequencies.[31] The C−H stretch spectral region contains valuable information about the alkyl chain conformation and geometry. The amplitude ratio (d^+/r^+) of the symmetric methylene (d^+, at ∼2850 cm^{-1}) and the symmetric methyl (r^+, at ∼2874 cm^{-1}) stretch vibrational modes is a common indicator for the conformation of alkyl chains.[32−35] A value of $d^+/r^+ \ll 1$ is associated with a stretched all-trans alkyl chain conformation, whereas a value of $d^+/r^+ > 1$ indicates that gauche defects dominate the measured SF spectra. When we compare the spectra, we focus on this d^+/r^+ ratio. d^+/r^+ ratios were obtained from a global fitting procedure,[33] in which the weak nonresonant background is taken into account by using a measured SF signal from an all-deuterated sample. This is done because the nonresonant background varies per oil/surfactant/water interface and polarization direction.

Differences in the spectral region above 2900 cm^{-1} are not immediately useful for determining the chain conformation[31,36] as it contains a number of modes that are not well-resolved, some of which consist of couplings to overtones. The methyl groups in the DTA^+ head group vibrate at higher frequencies:[37] The symmetric stretch mode appears at ∼2985 cm^{-1}, and the

dx.doi.org/10.1021/ja4120117 | J. Am. Chem. Soc. 2014, 136, 2040−2047

antisymmetric stretch mode appears at 3040 cm^{-1} in the Raman spectrum.[38] They do not influence our observed d^+/r^+ ratios. The antisymmetric stretch mode appears in our SF spectra as a very weak and broad feature at ~3045 cm^{-1}. Since the signal is very close to our detection limit, it cannot be used here. The DS^- head group does generate a strong signal (close to that of the pure sulfate ion[38]), and it has been used in conjunction with the C−H signal to determine an upper limit for the amount of surface adsorbed DS^-.[39]

To critically test whether or not a given charged amphiphile penetrates into or perturbs the liquid oil interface we have measured (i) the surface structures of DS^- ions and DTA^+ ions adsorbed on 150−250 nm diameter liquid deuterated oil nanodroplets, on impenetrable polytetrafluoroethylene (PTFE) and polystyrene (PS) particles, and (ii) the conformational changes of the oil surface molecules at the droplets by selectively deuterating the surfactant ions. Both bare particles do not generate SF signal in the C−H stretch region below 2900 cm^{-1} (as we confirmed experimentally).[40] Although the chemical structures of oil, PTFE, and PS are different, we use the three systems to compare surfactant alkyl chain conformations on a liquid (penetrable) and solid (impenetrable) interface. It is expected that if chain penetration plays an important role, the different state of matter (solid vs liquid) will be more important than the chemical differences such as between the PTFE and PS surfaces.

The following discussion begins with a description of our measurements of the structure of DS^- on PS and PTFE and DTA^+ on PTFE nanoparticles. Then, we follow the adsorption of both surfactants on d_{34}-hexadecane oil droplets. Next, we describe measurements performed using alkyl-deuterated surfactants in order to elucidate amphiphile-induced changes in the interfacial structure of the liquid oil droplets. We end with monitoring the changes in the electrokinetic mobility (representative of the interfacial charge) and water structure.

Amphiphile Chain Conformation. Figure 2 shows SFS spectra of the alkyl tails of DTA^+ ions on PTFE nanoparticles (A) and on d_{34}-hexadecane oil droplets (C), and of DS^- ions on PTFE and PS nanoparticles (B), and on d_{34}-hexadecane oil droplets (D). The particles/droplets were dispersed in solutions of SDS and DTAB in D_2O. The surfactant concentrations are given in the caption and are all below their respective cmc's. SF spectra of surfactants on the oil droplets are plotted in panels C and D, for two different concentrations. It can be seen in panels A and B that the spectra for the C_{12} alkyl chains of DTA^+ and DS^- on PTFE resemble each other closely, with both having very large d^+/r^+ ratios (3.6 and 4.5 for DTA^+ and DS^-, respectively). The spectra for DS^- ions on PTFE/PS and on the hexadecane oil droplet are also very similar (B,D), with d^+/r^+ amplitude ratios of 4.5 and 3.7, indicating the predominance of gauche defects on the spectra shown in panels A, B, and D. The spectra in panel C of DTA^+ on d-C_{16}, however, are clearly quite different from the others, with approximately equal amplitudes for both d^+ and r^+ modes, indicating that the alkyl chains have more all-trans character. The increasing SF intensity with increasing bulk concentrations in panels C and D indicates that more surfactant molecules adsorb to the interface when the bulk concentration is raised.

Thus, it is clear that the chain conformation for the DS^- alkyl chains is not very different on solid PTFE particles, PS particles, and liquid oil droplets. The chain conformation of DTA^+ ions, however, is very different on solid PTFE and liquid oil droplets.

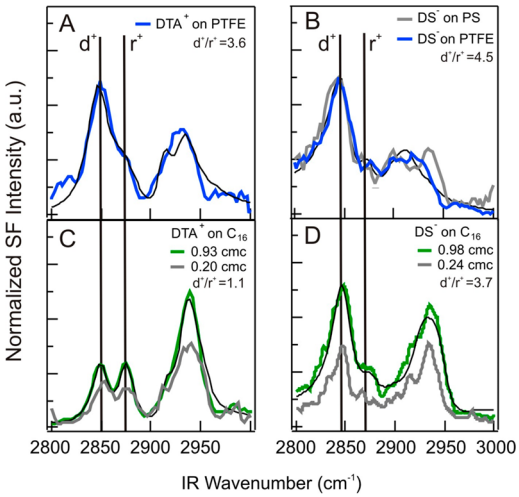

Figure 2. Comparison of the amphiphile structure on solid impenetrable and liquid penetrable interfaces. SFS spectra of the interface of impenetrable particles with solutions containing DTA^+ and DS^- ions showing the response of the alkyl chains of DTA^+ ions on PTFE particles (A, 0.93 cmc, 14 mM), and the response of the alkyl chains of DS^- ions on PTFE (blue trace) and PS particles (gray trace), both at total concentrations of 0.98 cmc, or 8 mM (B). Panel C shows SFS-spectra of the alkyl chains of DTA^+ ions at the interface of d_{34}-hexadecane droplets in solutions containing different total concentrations of DTA^+ (0.20 and 0.93 cmc or 3 and 14 mM). Panel D shows SFS spectra of the alkyl chains of DS^- ions at the interface of d_{34}-hexadecane droplets in solutions containing different total concentrations of DS^- (0.24 cmc and 0.98 cmc or 2 mM and 8 mM). The frequencies of the symmetric methylene (d^+, 2850 cm^{-1} and the symmetric methyl (r^+, 2874 cm^{-1}) stretch vibration are highlighted. All spectra are recorded in the C−H stretch frequency region using an SSP polarization combination. Here, SSP indicates that the sum frequency and visible (infrared) beams are polarized perpendicular (parallel) with respect the scattering plane. The black lines are fits from which the given d^+/r^+ amplitude ratios are derived.

This difference might stem from the fact that DTA^+ penetrates into the oil phase which would also result in a perturbed conformation of the interfacial oil molecules. In the following experiment, we will show that the oil phase is indeed perturbed by the presence of DTA^+ ions, but not detectably by the presence of DS^- ions. In the Supporting Information we compare the spectra to previously published work on related systems and relate the spectral shapes to possible chain conformations.

Oil Chain Conformation. Having measured the difference in alkyl chain conformation of DS^- and DTA^+ ions on the liquid oil drops, we now describe the response of the interfacial oil molecules to test whether their conformation is perturbed by the surfactant ions. Figure 3 shows SFS spectra of the C−H-stretch modes of h-hexadecane droplets dispersed in D_2O to which different bulk concentrations of alkyl chain deuterated d-DS^- (A, 0, 0.06, 0.25, 0.98 × cmc) and d-DTA^+ (B, 0.0, 0.03, 0.25, 0.93 × cmc) were added. The intensities can be compared within each panel, but not between panels, as the average droplet size and size distribution of these two sample series are different (which here influences the spectral intensity but not the spectral shape[41]). From Figures 2C−D it is clear that up to the cmc the interfacial coverage is increased if more surfactant is added to the solution. Figure 3A shows that adding d-DS^- does not detectably change the hexadecane SF spectra. This implies that, within our detection limit, no significant changes

dx.doi.org/10.1021/ja4120117 | J. Am. Chem. Soc. 2014, 136, 2040−2047

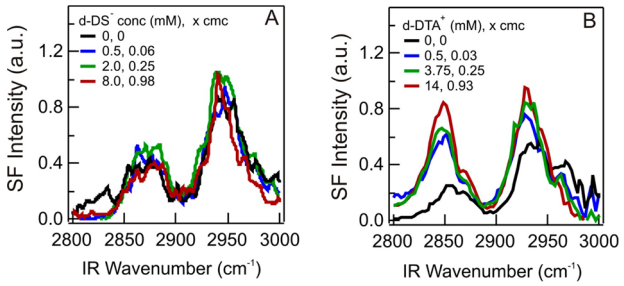

Figure 3. Effect of DS^- and DTA^+ ions on the interfacial structure of the oil phase. The graphs show SFS spectra in the CH-region of hexadecane nanodroplets in solutions containing various concentrations of DS^- (A, 0, 0.06, 0.25, 0.98 × cmc) and DTA^+ ions (B, 0, 0.03, 0.25, 0.98 × cmc) with deuterated alkyl chains. All spectra are recorded in SSP polarization combination. Intensities have not been scaled within each panel.

are observed in the interfacial oil chain conformations. Figure 3B shows that adding *d*-DTA^+ changes the hexadecane SF spectra significantly. The total spectral intensity and the d^+/r^+ ratio of the vibrational modes of the interfacial oil molecules increase with an increasing surface concentration of d-DTA^+ ions. Note that the spectra of the surfactant free samples ("0 mM") in panels A and B have the same shape to within the experimental error, as both have the same d^+/r^+ ratio to well within the 0.4 uncertainty in our d^+/r^+ ratio measurement (as we determined previously[42] from 11 different samples prepared and measured under identical conditions). These results clearly imply that the surface structure of the interfacial oil molecules is altered by the DTA^+ ions. No such conclusion can be drawn for the DS^- ions, however.

Electrostatic Properties. To determine the electrostatic properties of the interface, we performed electrokinetic mobility measurements.[43] Figure 4A displays the absolute

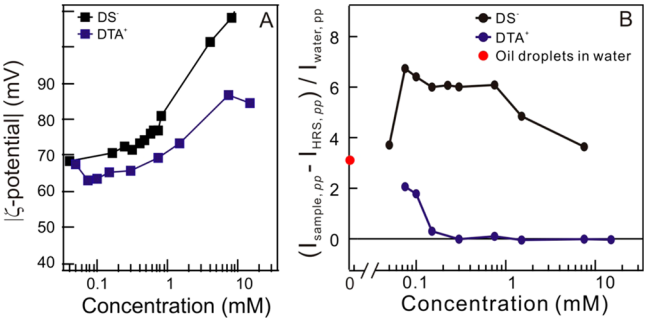

Figure 4. Interfacial ζ-potential and SHS response. The graphs show (A) the absolute values of the zeta potential for droplet solutions with different concentrations of DS^- and DTA^+, and (B) second harmonic scattering results for droplet solutions with different concentrations of SDS and DTAB. The scattering angle was 35°, and the polarization combination was set to PP (i.e., all beams are polarized along the horizontal scattering plane). The zeta potential for a surfactant free droplet solution is ∼−50 mV.

zeta potential for a solution of 0.01 v/v% hexadecane droplets in aqueous solutions against different concentrations of SDS and DTAB. It can be seen that for both solutions the zeta potential increases in magnitude, from +63 (0.005 × cmc) to +87 mV (0.93 × cmc) for DTA^+ and from −68 (0.006 × cmc) to −108 mV (0.93 × cmc) for DS^- with increasing surfactant concentration. The observation can be explained by an increase in the amount of surfactant at the oil/water interface (which agrees with the increasing SF signals of Figure 2C,D). The zeta potential of bare hexadecane droplets in ultrapure water is ∼−50 mV (not shown), a value that is in agreement with previous studies.[44]

Interfacial Water. The interfacial water around our nanoscopic droplets can be measured with second harmonic[45] (SH) scattering,[46−49] a process that occurs only in non-centrosymmetric regions. The SH signal reports on the difference in orientational directionality of the water molecules in the interfacial region compared to the orientational directionality of the bulk solution[45,50−52] (on a femtosecond time scale). The Supporting Information contains additional details on the origin of the signal. The change in directionality can be induced by chemical interactions (such as H-bonding), or by electrostatic interactions of the dc field from the surface ions that interact with the water dipoles in the surface region ("$\chi^{(3)}$ effect" as discovered by the Eisenthal lab[45]). Both effects can act together and give rise to SH electric field contributions that interfere constructively or destructively, which can lead to an increasing or decreasing SH intensity. Figure 4B displays the SH intensity obtained at a scattering angle of 35° in PP polarization (i.e., all beams polarized in the horizontal scattering plane), and around the angle of maximum intensity[53] for solutions with oil droplets and different concentrations of SDS and DTAB. The measured intensity was corrected for hyper Rayleigh scattering from the same solution without droplets, and then divided by the (isotropic) hyper Rayleigh scattering intensity in SS polarization of pure water for normalization purposes (following ref 54).

It can be seen that the SH intensity changes for both surfactants, but in a very different manner. For DS^- the intensity increases sharply (starting at 0.07 mM/8.6 × 10^{-3} × cmc), then levels off (0.1 mM/0.012 × cmc), and then drops again (1 mM/0.12 × cmc). For DTA^+ the intensity decreases sharply, and for concentrations greater than 0.3 mM (0.02 × cmc), there is no detectable difference between the SH intensity coming from the droplet solution and the droplet free solution. For both the zeta potential and SH intensity a similar trend is observed for DTAC, with the difference that the magnitude of the zeta potential increases to larger values, and the SH intensity vanishes at even lower concentrations.

The changes in the SH intensity originate from chemical or electrostatic changes in the interfacial region. Increasing the DS^- ion concentration increases both the number of sulfate groups as well as the magnitude of the electrostatic potential. With an increasing number of surface sulfate groups, the number of sulfate H-bonded water molecules also increases (as was shown in Figure 1). H-bonded water molecules have their dipoles oriented toward the sulfate ions. The presence of the alkyl chain most likely results in a larger number of H-bonded water molecules with their dipoles directed toward the surface plane. With an increasing electrostatic field that is directed toward the surface ions, more water molecules will have their dipoles oriented toward the surface. Thus, with an increasing concentration of SDS the H-bonding and the dc field increase the orientational directionality of the interfacial water in the same direction, both favoring water dipoles pointing toward the surface. The combination of both effects ensures that the coherent SH signal increases. The decreasing intensity beyond 0.12 × cmc can be explained by an increase in electrostatic screening:[45,50] because the increased ionic strength of the solution results in a more effective screening of the surface

dx.doi.org/10.1021/ja4120117 | J. Am. Chem. Soc. 2014, 136, 2040−2047

electric field, the amount of water that is orientationally affected decreases, and so does the SH intensity.

We now turn to the DTA^+ ions. From the Raman hydration-shell measurements (in Figure 1) it is likely that DTA^+ ions are surrounded by water molecules that have a similar Raman response as water molecules around hydrophobic solutes. When such ions adsorb to the interface, it may be expected that this results in a loss of water dipolar orientation along the surface normal. The adsorption of DTA^+ ions also results in a more positive surface potential, which will tend to orient some water molecules with their dipoles pointing away from the surface, resulting in a reduction of the orientational directionality compared to that of a surfactant free droplet. Since both the change in H-bond configuration and the positive surface charge change the initially present directionality of the water molecules adjacent to the neat oil/water interface, the SH field decreases. At higher concentrations one may also expect that electrostatic screening reduces the SH signal. However, since the SH signal is already below the detection limit, this is not observed. Thus, DS^- ions enhance the directionality of surface water molecules, while DTA^+ ions reduce the directionality of surface water molecules.

Interfacial Structural Implications. The above results reveal striking differences between the interfacial structure of anionic DS^- and cationic DTA^+ amphiphiles. Water molecules are H-bonded to DS^- sulfate head groups. Upon adsorbing to a hydrophobic/water interface the interfacial DS^- hydrophobic tails do not have very different chain conformations when adsorbed on either a solid or a liquid hydrophobic interface. They also do not detectably change the conformation of the surface oil molecules (as concluded from vibrational sum frequency spectroscopy data). The orientational directionality of the surface water is strongly increased with respect to the bare oil/water interface, which can be explained by H-bonding and electric field effects that orient water molecules in the same direction.

Water molecules around the DTA^+ ions have a structure similar to that around hydrophobic solutes. DTA^+ ions have a significantly different alkyl chain conformation when adsorbed on a liquid hydrophobic interface or on an impenetrable solid/water interface. DTA^+ strongly perturbs the structure of the oil molecules at the droplet/water interface. The orientational directionality of water compared to that at a neat oil/water interface is strongly reduced. Thus, DS^- and DTA^+ ions clearly interact very differently with water and the oil/water interface.

Schweighofer[55] et al. simulated a single SDS molecule on the water/air and water/CCl_4 interface and found that on the water/air interface the DS^- ion has the head group immersed in the water phase and the tail bent along the surface plane. Such a conformation is similar to the one that would give rise to the observed SF spectra in Figure 2. The DS^- ion on the CCl_4/water interface has an alkyl tail that is pointing into the oil phase under an angle. Such a tail structure would give rise to $d^+/r^+ < 1$ (see Supporting Information for more details, and this would not explain our results). In a subsequent study[56] Schweighofer et al. simulated SDS and a charge reversed equivalent on the CCl_4 water interface at high surfactant concentrations (0.45 nm^2/molecule). Here, the alkyl tails are immersed in the CCl_4 phase, and the positively charged head group is further down into the water phase than the negatively charged head group. Simulations by Abranko-Rideg[57] et al. simulated two different concentrations (1.66 nm^2/molecule and 0.45 nm^2/molecule) of DS^- and DTA^+ on the air/water interface and found that at lower concentrations the head groups penetrate deeper into the water phase. Furthermore, they found that the sulfate head group is immersed somewhat deeper than the trimethyl ammonium head group. This finding is in agreement with our results. Simulations by Vacha[58] were done of DS^- at decane/water and air/water interfaces at low concentrations (1.0 nm^2/molecule). It was found that air/water and decane/water interfaces are very different with the air/water interface displaying surfactant aggregation, in contrast to the decane/water interface, which displayed no aggregation. The DS^- head groups distort the water orientational distribution down to a distance of ~3.5 nm away from the Gibbs dividing plane. From an experimental point of view it is further interesting to note that it is not possible to generate stable CCl_4/water emulsions with only SDS or DTAB. Thus, our results are partly in agreement with simulations, but since complete oil nanodroplets cannot be simulated in water and an explanation for the large negative electrokinetic potential[59] is yet to be found, comparisons are probably not definitive.

Interfacial Stabilization. It is interesting to consider the relationship between the remarkably different interfacial structures of the above cationic and anionic amphiphiles, the concentration dependence of the interfacial structure, and the resulting different molecular mechanisms by which they might lower the interfacial free energy of the oil/water interface. Anionic DS^- amphiphiles are directly H-bonded, and decorate the oil/water interface with hydrated sulfate groups. The water orientational directionality also increases when more surfactants adsorb. The oil structure on the other hand does not display detectable changes. Thus, water is likely to play a major role in the stabilization of the interface. The cationic DTA^+, on the other hand, is very weakly hydrated, and when it is added to the interface, the conformational flexibility of the oil changes. The water structure changes as well, but the orientational directionality is decreased. Thus, the molecular actors have different roles in both surface structures and are concentration dependent, and consequently the molecular mechanism by which the interfacial energy is lowered might also be different. This difference could be verified by additional temperature dependent measurements and/or molecular dynamics simulations performed to elucidate entropic, energetic, and molecular contributions to the corresponding amphiphile stabilized surface free energy.

The finding that charged amphiphiles with different head group structures might have different roles in both surface structures, and consequently in surface stabilization, is of chemical importance in, e.g., nanosynthesis and emulsification. In biochemistry it has consequences for vesicle and membrane assembly, protein/peptide folding, aggregation, and stabilization.

■ CONCLUSIONS

By combining hydration-shell Raman spectroscopy, vibrational sum frequency scattering, electrokinetic mobility, and second harmonic scattering measurements, we have discovered the strong influence of specific ion−water interactions on the structure of surfactant stabilized oil/water interfaces. The weakly hydrated DTA^+ surfactant has a different conformation on the oil droplet/water interface than on an impenetrable solid hydrophobic particle/water interface. In addition, DTA^+ induces a change in the oil surface structure. The surface water structure changes as well, displaying a reduction in the number of water molecules whose dipoles are orientationally

directed along the surface normal, up to the point where no detectable difference with the bulk solution exists (at 0.02 × cmc). In contrast, the strongly hydrated DS^- surfactant has a very similar chain conformation on the impenetrable solid hydrophobic particle/water interface and on the oil droplet/water interface. At the same time, it does not induce a detectable change in the oil surface structure. The surface water structure changes significantly, displaying a growing number of water molecules that are orientationally directed along the surface normal. The results further suggest a difference between the interfacial stabilization mechanisms of the two surfactants, with the strongly hydrated anionic surfactant group mostly stabilizing the interfacial water and the weakly hydrated cationic surfactant mostly stabilizing the interfacial oil.

MATERIALS AND METHODS

n-Hexadecane ($C_{16}H_{34}$, 99.8%, Sigma-Aldrich), *h*-DTAB (99%, Sigma-Aldrich), d_{34}-hexadecane ($C_{16}D_{34}$, 98% *d*, Cambridge Isotope), *d*-SDS (99% *d*, Cambridge Isotope), *d*-DTAB (99% *d*, Cambridge Isotope), and D_2O (99%, Sigma-Aldrich) were used as received. *h*-SDS (99%, Biomol) was purified by multiple recrystallizations. Glassware was cleaned with a 3/7 H_2O_2/H_2SO_4 solution, after which it was thoroughly rinsed with ultrapure water (0.053 μS/cm,TKA). Aqueous solutions of sodium bromide (NaBr, 98.52%, J.T. Baker), trimethyloctylammonium bromide (OTA^+, ≥ 98.0%, Aldrich), and sodium octylsulfate (SOS, ∼95% Sigma) with a concentration of 0.1 M were prepared using ultrapurified water (Milli-Q UF plus, Millipore, Inc., electrical resistance of 18.2 MΩ cm)

Dispersions of oil nanodroplets in water were prepared with 2 v/v % of hexadecane or d_{34}-hexadecane in D_2O. The solutions were mixed for 4 min with a hand-held homogenizer (TH, OMNI International) and subsequently placed in an ultrasonic bath (35 kHz, 400 W, Bandelin) for the same duration. The resultant stock emulsion was then diluted with a solution of DTAB or SDS in D_2O to yield the desired surfactant concentration. The size distribution of the droplets was measured with dynamic light scattering (DLS, Malvern ZS nanosizer) and consistently found to have a mean diameter in the range 150−250 nm with a polydispersity index (PDI) of less than 0.2. The PTFE particles were synthesized by J. Leutzenkirchen according to the procedure described by Preocanin et al.[60] The particles had a mean diameter of 235 nm with a PDI of 0.1. They were dispersed in 1 mL of a solution of 8 mM h-SDS (14 mM h-DTAB) in D_2O. The final volume fraction was 1.17 (1.3)%. Bare polystyrene particles were purchased from Polysciences, had a mean radius of 246 nm (PDI 0.08), and were used at a volume fraction of 1%.

Raman spectra were collected using an Ar-ion laser (514.5 nm) as the excitation source with approximately 15 mW of power at the sample. Duplicate spectra were collected with an integration time of 5 min. The backscattered Raman photons were collected and delivered at the entrance slit of a 300 gr/mm-grating using a fiber bundle consisting of seven 100 μm core diameter fibers (arranged in a close packed circular array at the collection end and a linear stack at the entrance slit). The spectral resolution of the Raman system is ∼1 nm (∼25 cm^{-1} or ∼4 CCD pixels), as determined from the full-width-at-half-maximum of isolated neon calibration lamp lines measured using the same collection fiber-bundle and detection system. All Raman spectra are unpolarized (as they include both S and P polarized scattering). Previous studies have shown the corresponding S and P components and SC of hydrophobic and ionic solutes.[11−13] The Raman-MCR decomposition of measured spectra into SC and pure water components was performed using self-modeling curve resolution (SMCR).[61] Although SMCR is limited to two component systems, we have previously shown that multicomponent systems can be reduced to two components by varying the concentration of only one component.[12,14b] The strategy has been used in the present studies by including the same Br^- concentration in both solvent (as Na^+Br^-) and OTA^+ surfactant solutions (as OTA^+Br^-). Note that the OH band of water molecules around Na^+ ions is virtually indistinguishable from that of pure water,[13] and thus, Na^+ ions have essentially no influence on the above SC spectra, or those obtained from OS^-Na^+ surfactant solutions (with salt-free water as the solvent).

Second harmonic scattering measurements were performed, as previously described in detail,[49] using 190 fs laser pulses centered at 1028 nm with a 200 kHz repetition rate. The polarized pulses were focused into a cylindrical glass sample cell (4.2 mm inner diameter). The scattered SH light was collimated with a plano-convex lens (f = 5 cm) and then sequentially passed through an iris to control the angular resolution and a bandpass filter. The filtered SH light was focused into a PMT by a plano-convex lens (f = 3 mm). The gate width of the PMT was 10 ns, and the acquisition time was 1 s. A quarter-wave plate, a half-wave plate, and a linear polarizer were used to control the polarization of the incoming fundamental beam. The polarization of the scattered light was analyzed with another polarizer. The SH signals were measured at a scattering angle of 35° with an angular resolution of ±1.75°. The plotted data points represent the SHS signal corrected for background hyper Rayleigh scattering and are normalized to the SS signal of neat water:

$$\frac{I(\theta = 35)_{\mathrm{SHS,droplets,PP}} - I(\theta = 35)_{\mathrm{HRS,solution,PP}}}{I(\theta = 35)_{\mathrm{HRS,SS}}}$$

The error in the reproducibility of the SHS measurements is 1−2%.

Vibrational SFS spectra were measured, as previously described in detail[62,63] using broadband infrared (IR) laser pulses centered at 2900 cm^{-1} (fwhm =120 cm^{-1}) and visible (VIS) pulses at 800 nm (fwhm = 12 cm^{-1}) at a repetition rate of 1 kHz. The focused laser beams were overlapped under an angle of 20° in a sample cuvette with a path length of 200 μm. At a scattering angle of 60°, the scattered SF light was collimated using a plano-convex lens (f = 15 mm, Thorlabs LA1540-B) and passed through two short wave pass filters (Third Millenium, 3RD770SP). The SF light was spectrally dispersed with a monochromator (Acton, SpectraPro 2300i) and detected with an intensified CCD camera (Princeton Instruments, PI-Max3) using a gate width of 10 ns. The acquisition time for a single spectrum was set between 150 and 300 s. A Glan-Taylor prism (Thorlabs, GT15-B), a half-wave plate (EKSMA, 460−4215), and a polarizing beam splitter cube (CVI, PBS-800−050) and two BaF_2 wire grid polarizers (Thorlabs, WP25H-B) were used to control the polarization of the SFG, VIS, and IR beams, respectively. All shown SFS spectra were normalized by an SFG spectrum obtained in reflection geometry from a z-cut quartz crystal. Concentration series were measured against a reference sample that was inserted between every other measurement, to detect and correct for possible fluctuations during the course of the experiment.

d^+/r^+ ratios were obtained from a global fitting procedure, in which the weak nonresonant background is taken into account by using a measured SFG signal from an all-deuterated sample. This is done because the nonresonant background varies per sample and polarization direction. The details are described in ref 42. The error bar on the given d^+/r^+ ratios is ∼0.4, and increases for larger d/r ratios since smaller signals are more prone to errors when they approach the detection limit of our system. Spectra taken from the same droplet/particle solution can be compared in intensity (e.g., spectra in Figure 2C,D, and 3A,B), while different solutions cannot (e.g., Figure 2, part C, with part D), since the particle/droplet size and its distribution might vary as well as the volume fraction (and the SF signal is very sensitive to that[26]). For this reason the spectra are normalized.

ASSOCIATED CONTENT

Supporting Information

Relationship between the SFG signal and the molecular conformation of DS^- surfactant alkyl chains, and more details regarding the interpretation of the origin of the SH intensity. This material is available free of charge via the Internet at http://pubs.acs.org.

AUTHOR INFORMATION

Corresponding Author

sylvie.roke@epfl.ch

Notes

The authors declare no competing financial interest.

ACKNOWLEDGMENTS

This work is supported by the Julia Jacobi Foundation, the Swiss National Science Foundation (Grant 200021_140472), the European Research Council (G 240556), and the National Science Foundation (Grant CHE-1213338). We thank J. Luetzenkirchen for generously providing the PTFE particles.

REFERENCES

(1) Collins, K. D.; Washabaugh, M. W. *Q. Rev. Biophys.* **1985**, *18*, 323.

(2) Jungwirth, P.; Tobias, D. J. *Chem. Rev.* **2006**, *106*, 1259.

(3) Kunz, W. *Specific Ion Effects*; World Scientific Publishing Company: Singapore, 2009.

(4) Kunz, W.; Nostro, P. L.; Ninham, B. W. *Curr. Opin. Colloid Interface Sci.* **2004**, *9*, 1.

(5) Gurau, M. C.; Lim, S.-M.; Castellana, E. T.; Albertorio, F.; Kataoka, S.; Cremer, P. S. *J. Am. Chem. Soc.* **2004**, *126*, 10522.

(6) It should be mentioned here that all chemicals used, even if they are purified maximally, can still be expected to contain an impurity concentration in the order of 1 to several micromolar. Assuming the surface affinity of an impurity will be constant for a planar surface or a particle surface, it can easily be seen that increasing the surface area contained in a fixed volume will decrease the inherent surface density of surface impurities (since the concentration is finite). Thus, use of a sample with a 1 vol % concentration of 100 nm droplets greatly reduces the unwanted effects of impurities compared to a sample with a planar interface (and the same bulk volume of chemicals). We have used SFS experiments to determine the effect of impurities and concluded that at least 97% of the droplet surface is clean.

(7) Jena, K. C.; Scheu, R.; Roke, S. *Angew. Chem., Int. Ed.* **2012**, *51*, 12938.

(8) Fega, K. R.; Wilcox, D. S.; Ben-Amotz, D. *Appl. Spectrosc.* **2012**, *66*, 282.

(9) Perera, P. N.; Fega, K. R.; Lawrence, C.; Sundstrom, E. J.; Tomlinson-Phillips, J.; Ben-Amotz, D. *Proc. Natl. Acad. Sci. U.S.A.* **2009**, *106*, 12230.

(10) Gierszal, K. P.; Davis, J. G.; Hands, M. D.; Wilcox, D. S.; Slipchenko, L. V.; Ben-Amotz, D. *J. Phys. Chem. Lett.* **2011**, *2*, 2930.

(11) Davis, J. G.; Gierszal, K. P.; Wang, P.; Ben-Amotz, D. *Nature* **2012**, *491*, 582.

(12) Davis, J. G.; Rankin, B. M.; Gierszal, K. P.; Ben-Amotz, D. *Nat. Chem.* **2013**, *5*, 796.

(13) Perera, P. N.; Browder, B.; Ben-Amotz, D. *J. Phys. Chem. B* **2009**, *113*, 1805.

(14) (a) Rankin, B. M.; Hands, M. D.; Wilcox, D. S.; Fega, K. R.; Slipchenko, L. V.; Ben-Amotz, D. *Faraday Discuss.* **2013**, *160*, 255. (b) Rankin, B. M.; Ben-Amotz, D. *J. Am. Chem. Soc.* **2013**, *135*, 8818. (c) Wilcox, D. S.; Rankin, B.; Ben-Amotz, D. *Faraday Discuss.* **2013**, *167*, 177.

(15) Mukerjee, P.; Mysels, K. J. *NSRDS-NBS,* 1971, *36*.

(16) Lu, J. R.; Marrocco, A.; Su, T. J.; Thomas, R. K.; Penfold, J. *J. Colloid Interface Sci.* **1993**, *158*, 303.

(17) Schlossman, M. L.; Tikhonov, A. M. *Annu. Rev. Phys. Chem.* **2008**, *59*, 153.

(18) Sloutskin, E.; Sapir, Z.; Bain, C. D.; Lei, Q.; Wilkinson, K. M.; Tamam, L.; Deutsch, M.; Ocko, B. M. *Phys. Rev. Lett.* **2007**, *99*, 136102.

(19) Staples, E.; Penfold, J.; Tucker, I. *J. Phys. Chem. B* **2000**, *104*, 606.

(20) Zarbakhsh, A.; Webster, J. R. P.; Eames, J. *Langmuir* **2009**, *25*, 3953.

(21) Conboy, J. C.; Messmer, M. C.; Richmond, G. L. *J. Phys. Chem. B* **1997**, *101*, 6724.

(22) de Aguiar, H. B.; de Beer, A. G. F.; Strader, M. L.; Roke, S. *J. Am. Chem. Soc.* **2010**, *132*, 2122.

(23) Knock, M. M.; Bell, G. R.; Hill, E. K.; Turner, H. J.; Bain, C. D. *J. Phys. Chem. B* **2003**, *107*, 10801.

(24) Messmer, M. C.; Conboy, J. C.; Richmond, G. L. *J. Am. Chem. Soc.* **1995**, *117*, 8039.

(25) Wilkinson, K. M.; Qunfang, L.; Bain, C. D. *Soft Matter* **2006**, *2*, 66.

(26) Roke, S.; Gonella, G. *Annu. Rev. Phys. Chem.* **2012**, *63*, 353.

(27) Lambert, A. G.; Davies, P. B.; Neivandt, D. J. *Appl. Spectrosc. Rev.* **2005**, *40*, 103.

(28) Zhuang, X.; Miranda, P. B.; Kim, D.; Shen, Y. R. *Phys. Rev. B* **1999**, *59*, 12632.

(29) Roke, S. *ChemPhysChem* **2009**, *10*, 1380.

(30) Vidal, F.; Tadjeddine, A. *Rep. Prog. Phys.* **2005**, *68*, 1095.

(31) Tyrode, E.; Hedberg, J. *J. Phys. Chem. C* **2012**, *116*, 1080.

(32) Beattie, D. A.; Haydock, S.; Bain, C. D. *Vib. Spectrosc.* **2000**, *24*, 109.

(33) de Aguiar, H. B.; Strader, M. L.; de Beer, A. G. F.; Roke, S. *J. Phys. Chem. B* **2011**, *115*, 2970.

(34) Esenturk, O.; Walker, R. A. *J. Chem. Phys.* **2006**, *125*, 174701.

(35) Guyot-Sionnest, P.; Hunt, J. H.; Shen, Y. R. *Phys. Rev. Lett.* **1987**, *59*, 1597.

(36) Wang, H. F.; Gan, W.; Lu, R.; Rao, Y.; Wu, B. H. *Int. Rev. Phys. Chem.* **2005**, *24*, 191.

(37) Tyrode, E.; Rutland, M. W.; Bain, C. D. *J. Am. Chem. Soc.* **2008**, *130*, 17434.

(38) Jubb, A. M.; Allen, H. C. *J. Phys. Chem C* **2012**, *116*, 9085.

(39) de Aguiar, H. B.; de Beer, A. G. F.; Strader, M. L.; Roke, S. *J. Am. Chem. Soc.* **2010**, *132*, 2122.

(40) Posner, R.; Jubb, A. M.; Frankel, G. S.; Stratmann, M.; Allen, H. C. *Electrochim. Acta* **2012**, *76*, 34.

(41) de Beer, A. G. F.; Roke, S. *J. Chem. Phys.* **2010**, *132*, 234702.

(42) de Aguiar, H. B.; Strader, M. L.; de Beer, A. G. F.; Roke, S. *J. Phys. Chem. B* **2011**, *115*, 2970.

(43) Hunter, R. J. *Zeta Potential in Colloid Science*; Academic Press: Sidney, 1981.

(44) Creux, P.; Lachaise, J.; Graciaa, A.; Beattie, J.; Djerdjev, A. *J. Phys. Chem. B* **2009**, *113*, 14146.

(45) Ong, S.; Zhao, X.; Eisenthal, K. B. *Chem. Phys. Lett.* **1992**, *191*, 327.

(46) Wang, H.; Yan, E. C. Y.; Borguet, E.; Eisenthal, K. B. *Chem. Phys. Lett.* **1996**, *259*, 15.

(47) Yan, E. C. Y.; Liu, Y.; Eisenthal, K. B. *J. Phys. Chem. B.* **1998**, *102*, 6331.

(48) Schurer, B.; Hoffmann, M.; Wunderlich, S.; Harnau, L.; Peschel, U.; Ballauff, M.; Peukert, W. *J. Phys. Chem. C* **2011**, *115*, 18302.

(49) Gomopoulos, N.; Luetgebaucks, C.; Sun, Q.; Roke, S. *Opt. Express* **2013**, *21*, 815.

(50) Jena, K. C.; Covert, P. A.; Hore, D. K. *J. Phys. Chem. Lett.* **2011**, *2*, 1056.

(51) Petersen, P. B.; Saykally, R. J. *J. Phys. Chem. B* **2006**, *110*, 14060.

(52) Scheu, R.; Chen, Y.; Subinya, M.; Roke, S. *J. Am. Chem. Soc.* **2013**, *135*, 19330.

(53) de Beer, A. G. F.; Campen, R. K.; Roke, S. *Phys. Rev. B* **2010**, *82*, 235431.

(54) Schürer, B.; Wunderlich, S.; Sauerbeck, C.; Peschel, U.; Peukert, W. *Phys. Rev. B* **2010**, *82*, 241404.

(55) Schweighofer, K. J.; Essmann, U.; Berkowitz, M. *J. Phys. Chem. B* **1997**, *101*, 3793.

(56) Schweighofer, K. J.; Essmann, U.; Berkowitz, M. *J. Phys. Chem. B* **1997**, *101*, 10775.

(57) Abranko-Rideg, N.; Darvas, M.; Horvai, G.; Jedlovszky, P. *J. Phys. Chem. B* **2013**, *117*, 8733.

(58) Vácha, R.; Roke, S. *J. Phys. Chem. B* **2012**, *116*, 11936.

(59) Vacha, R.; Rick, S. W.; Jungwirth, P.; de Beer, A. G. F.; de Aguiar, H. B.; Samson, J. S.; Roke, S. *J. Am. Chem. Soc.* **2011**, *133*, 10204.
(60) Preocanin, T.; Selmani, A.; Lindqvist-Reis, P.; Heberling, F.; Kallay, N.; Lützenkirchen, J. *Colloids Surf., A* **2012**, *412*, 120.
(61) Lawton, W. H.; Sylvestre, E. A. *Technometrics* **1971**, *13*, 617.
(62) de Aguiar, H. B.; Samson, J.-S.; Roke, S. *Chem. Phys. Lett.* **2011**, *512*, 76.
(63) de Aguiar, H. B.; Scheu, R.; Jena, K. C.; de Beer, A. G. F.; Roke, S. *Phys. Chem. Chem. Phys.* **2012**, *14*, 6826.